arXiv:1406.6377v2 [cond-mat.other] 27 Jun 2014

Dissipative phase locking of exciton-polariton condensates

H. Ohadi,[1,*] R. L. Gregory,[1] T. Freegarde,[1] Y. G. Rubo,[2] A. V. Kavokin,[1,3] and P. G. Lagoudakis[1]

[1] *School of Physics and Astronomy, University of Southampton, Southampton, SO17 1BJ, United Kingdom*

[2] *Instituto de Energías Renovables, Universidad Nacional Autónoma de México, Temixco, Morelos, 62580, Mexico*

[3] *Spin Optics Laboratory, St. Petersburg State University, 1, Ulianovskaya, St. Petersburg, 198504, Russia*

Abstract

We demonstrate, both experimentally and theoretically, a new phenomenon: the presence of dissipative coupling in the system of driven bosons. This is evidenced for a particular case of externally excited spots of exciton-polariton condensates in semiconductor microcavities. We observe that for two spatially separated condensates the dissipative coupling leads to the phase locking, either in-phase or out-of-phase, between the condensates. The effect depends on the distance between the condensates. For several excited spots, we observe the appearance of spontaneous vorticity in the system.

Exciton-polaritons (polaritons) are bosonic quasiparticles formed by the strong coupling of photons in a Fabry-Perot microcavity with excitons in a semiconductor quantum well [1]. Due to their finite lifetime, polaritons need to be externally pumped. Once the income rate of polaritons exceeds their decay rate (i.e. the threshold), a condensate with macroscopic occupation is formed [2–5]. Condensation of exciton-polaritons is an example of a spontaneous symmetry breaking process in a many-body system [6–8]. Being externally driven, polaritons can condense in one or several quantum states out of thermal equilibrium [9], in contrast to atomic Bose-Einstein condensates [10, 11]. Once polaritons are condensed they flow out of the pump spots and experience an increase in in-plane momentum due to their repulsion from hot excitons in the reservoir and other polaritons [12–14]. The outflowing polaritons may couple and phase lock the spatially separated condensates [15]. The coupling mechanism has been attributed to the coherent "ballistic coupling" mechanism, whereby each condensate center is resonantly pumped by the outflow from the neighboring condensates.

Here, we investigate in detail the coupling mechanism of spatially separated condensates using a simple two-condensate geometry and find that the coherent "ballistic coupling" picture is inadequate in describing the phase locking of spatially separated polariton condensates. We show how two condensates could phase lock in symmetric or antisymmetric states depending on their separation distance, as well as their outflowing condensate wavevectors. Using an incoherent coupling mechanism, to which we refer as *dissipative coupling* here, we explain this behavior and generalize it to any array geometry in particular a triangular condensate array. We show experimentally and theoretically how dissipative coupling could result in macroscopic pure states where all condensates are in phase or nontrivial mixed states where adjacent condensates have $\pm 2\pi/3$ phase difference giving rise to the spontaneous appearance of vortices at the center of the array, where the condensates overlap.

We create polariton condensates by nonresonant pulsed excitation in a semiconductor microcavity (see Supp. Info. I A). By studying the near-field photoluminescence (PL) spectra of the cavity we can measure the phase and the momentum of the polaritons in each condensate. A condensate array is created with each excitation pulse by means of optical shaping of the pump beam. To gain more insight into the phase locking mechanism, we study the simplest case of a pair of condensates. Fig. 1 shows the time-integrated real space PL of a condensate pair at different spatial separations. The pattern resembles the interference pattern of two phase-locked cylindrical waves with wavevectors equal to the in-plane wavevector of free polariton eigenmodes resonant in frequency with the condensates [16]. The appearance of an interference pattern indicates that the condensate pairs are phase-locked at zero or π phase difference depending on their separation or outflow in-plane wavevector. The phase difference has a nearly periodic dependence on the product of the condensate pair separation and the wavevector of outflowing polaritons (k_c), as shown in Fig. 2 by blue and

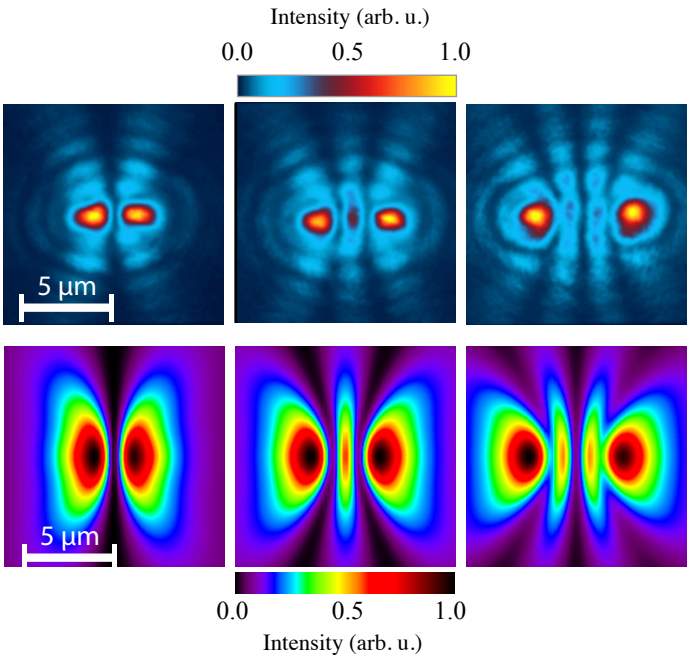

Figure 1. (upper row) The time-integrated images of two polariton condensates in real space at various separation. The condensates were created simultaneously at $P \simeq P_{th}$, where P_{th} is the threshold power for condensation. The observation of an interference pattern between the two condensates indicates that they are phase correlated. Zero intensity of the interference pattern in the middle of the two sources indicates that the two condensates are anti-synchronized. (lower row) The time-integrated GP simulations with random initial phase for 75 realizations at separation distances between the condensates as in the experiment is shown. The condensates phase lock on average to zero or π phase difference depending on their separation distance.

red dots (see also Supp. Fig. S2 and Video S1). Their relative phase changes abruptly as a function of the distance, which is untypical for the conventional Josephson coupling [17]. The coherent coupling mechanism requires in-phase coupling when the separation between two condensates is smaller than half the in-plane wavelength of the condensate (π/k_c), as shown by the dashed lines in Fig. 2. This is opposite to what we observe and also opposite to what our Gross-Pitaevskii simulations reveal (see Supp. Fig. S5).

The phase-locking mechanism can be understood if we consider condensation as an inherently dissipative and symmetry breaking process. Since the excitation is nonresonant, the phase coherence from the laser is lost and polaritons are initially created with random phases uniformly distributed across the pump spot. Due to phase fluctuations at the onset of condensation, this phase symmetry breaks down, and a macroscopic phase is built up along the whole condensate. One must consider the evolution of the unified wave function for both condensates, which naturally includes their interaction as they expand and interfere

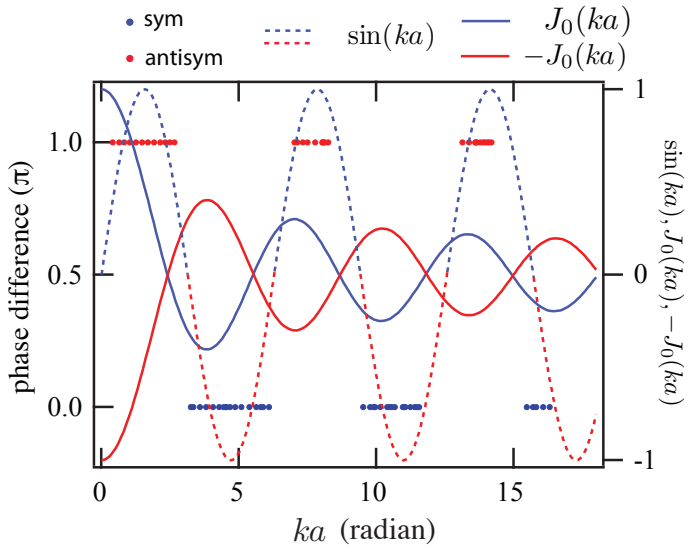

Figure 2. The condensates flip from symmetric to antisymmetric state as their separation (a) and outflow polariton in-plane wavevector (k_c) changes. The red circles show the antisymmetric and the blue circles show the symmetric states (see also Video S1). The solid curves are the calculated losses due to emission of free polaritons for symmetric (blue) and antisymmetric (red) states versus the unitless parameter $k_c a$. The dashed line which is plotting $\sin(k_c a)$ shows how the phase difference will behave if the coupling is coherent; the blue dashed lines are for symmetric phase locking and red for antisymmetric.

with each other. Condensed polaritons are repelled and ejected from the condensates with a specific in-plane wavevector k_c because of the interactions with each other and more importantly with the excitons in the reservoir [18] (see also Supp. Fig. S4). There are two types of losses from the condensates centers: (i) cavity losses through the Bragg mirrors counted by polaritons' radiative decay rate which could result in the radiative coupling of individual condensates [19], and (ii) losses due to the in-plane flow of polaritons with the wavevector k_c away from the excitonic reservoir, which is discussed here. Outflowing polaritons from different condensates can interfere constructively or destructively depending on the phases that they gain during their flow. The configurations which provide a destructive interference between the outflowing polaritons result in lower losses of polaritons from the condensates and higher polariton occupation numbers. This is amplified by stimulated scattering of polaritons from the reservoirs, which eventually leads to phase locking of condensates. In other words, interference between the two condensates breaks their individual phase symmetries to a state with the maximum wave function occupation number. Because the interference depends on the phase gained during the flow from one condensate to another, the phase relation between these phase-locked condensates depends on their positions or more generally on their topology as well as on the in-plane wavevector of outflowing polaritons. This

coupling mechanism is similar to the phase locking of Huygens's clocks [20, 21]. If the two clocks pendulums swing in in-phase mode, they tend to push the frame in the same direction resulting in frictional forces that eventually dampen the motion of the pendulums. If they swing in anti-phase mode the back actions cancel out and the frame does not move, minimizing the dissipative losses. The same mechanism is responsible for the sustained aftersound of the pianoforte [22]. The dissipative mechanism due to interference also closely resembles two radiating dipoles, where the loss (power dissipation) depends on their relative phase and separation [23]. In our system dissipation is governed by the interference of bosons outflowing from the condensates' centers.

The dependence of the total losses of two condensates on the phase difference θ between the individual condensates is given by

$$I(k_c a, \theta) \propto [1 + J_0(k_c a)\cos(\theta)], \tag{1}$$

where J_0 is the Bessel function (see Supp. Info. I C). This simple relation defines the dependence of the total losses of the polariton condensates on the phase difference between the individual condensates. At the formation of the condensates, the phase symmetry is spontaneously broken to a state that maximizes the total occupation number, which is a state that minimizes the losses. The blue and red solid lines in Fig. 2 shows the calculated losses of the condensates ($I(k_c a, \theta)$) for symmetric and antisymmetric states versus separation between the two condensates respectively. At each separation, the condensates pick on average the state with lower losses and flip between in-phase and anti-phase states in a nearly periodic fashion as their separation changes. The lower panel in Fig. 1 shows the 2D GP simulations with random initial conditions which is coupled to a hot exciton reservoir excited by the nonresonant pump [13]. Each figure is a time-integrated average of 75 realizations. The fringes between the condensates are due to interference between condensates that are phase locked on average in either zero or π phase difference. The phase difference depends on their separation and in-plane wavevector as the result of the phase symmetry breaking at the onset of condensation.

We observe a transition from the in-phase state to the out-of-phase state in time. By increasing the pump power to nearly twice the threshold power, we form condensates at a higher energy and larger in-plane wavevectors. We perform time-resolved interferometry of the two condensates by interfering the PL from one condensate with that from the other one using an actively stabilized Michelson interferometer in a mirror-retroreflector configuration (for details see Ref. 2 and Supp. Fig. S1). From the interferograms we can extract the time-resolved relative phase between them (see also Video S2). Fig. 3(a) shows the interference fringes just after the condensation. Initially, the two condensates anti-synchronize (π out of

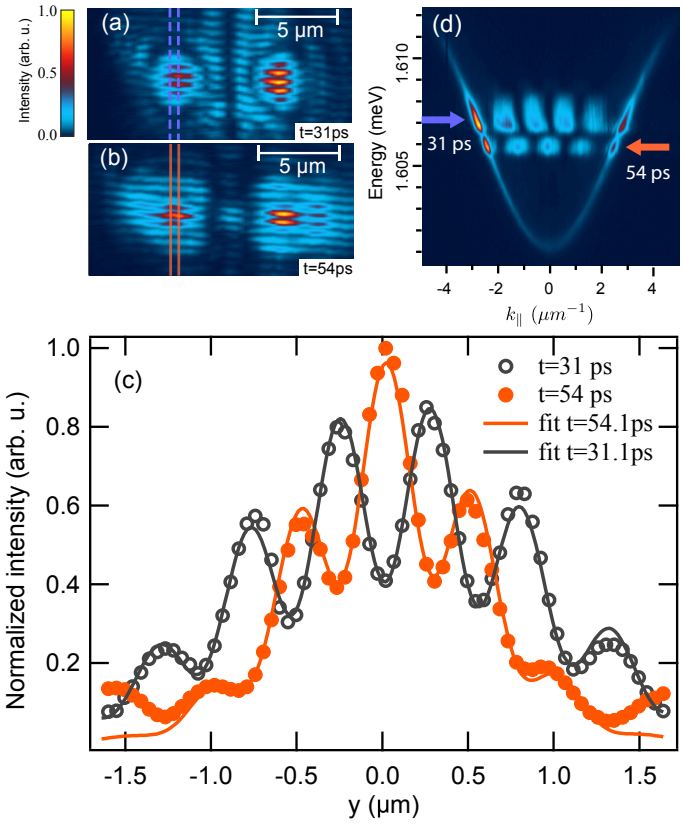

Figure 3. (a,b) The time-resolved interferograms at different times showing the phase synchronization of the two condensates. At early times and before condensation, they are not phase locked. When the condensates are formed they anti-synchronize (a) and as they relax in energy they synchronize (b). (c) The intensity profile of the interferograms at the position marked by the vertical lines in (a) and (b) at different times. The phase difference between the two condensates changes by π as they relax down in energy. The solid lines are the fits of a Gaussian function convoluted with a $\cos(ky + \phi)$, giving a phase difference of $(0.98 \pm 0.01) \times \pi$ between the two states. (d) The time-integrated momentum space is showing that condensation occurs at higher energies, with a gradual energy relaxation as time passes. At $t = 31\,\text{ps}$ (marked by a blue arrow) the two condensates are anti-phase synchronized and they synchronize in phase at $t = 54\,\text{ps}$ (marked by an orange arrow).

phase). As they relax in energy by phonon and exciton scatterings, they desynchronize and resynchronize at a later time [Fig. 3(b)]. However, when the two condensates resynchronize their phase difference changes by π [blue and orange line in Fig. 3(c)]. The symmetry flipping can also be seen in the momentum space images shown in Fig. 3(d). The condensates first anti-synchronize at a high energy marked by the blue arrow ($t = 31\,\text{ps}$) and then synchronize at a later time ($t = 54\,\text{ps}$) marked by the orange arrow.

Fig. 4(a,b) show the spectral tomography images of an equilateral triangular condensate

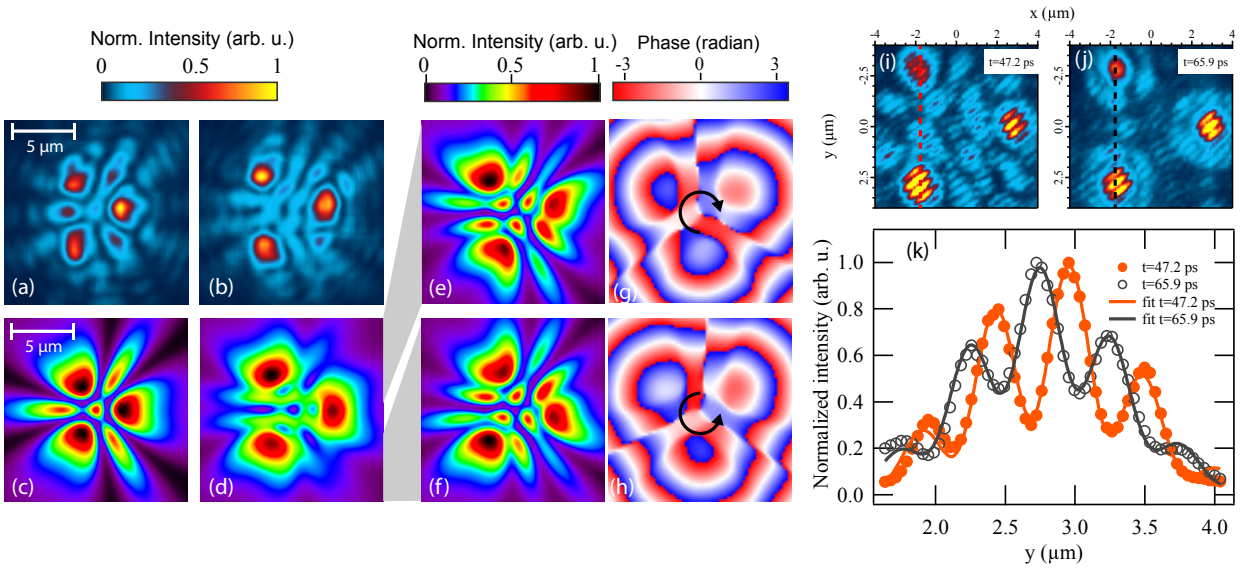

Figure 4. (a-d) Time-integrated real-space tomography images of the triangular array condensates are shown for $a = 4\,\mu$m (a), $a = 5.5\,\mu$m (b). (c,d) The GP simulations with random initial phase, averaged over 75 realizations at different separations matching the experimental conditions are shown. In (c) all three condensates are in phase but (d) is a mixture of vortices with ± 1 winding numbers shown in (e) and (f). The phase diagrams of (e) and (f) are shown in (g) and (h) proving that they are indeed vortex states with winding numbers of $+1$ (h) or -1 (g). (i,j) The time resolved interferograms resulted from the interference of two condensates with each other are shown at $t = 47.2\,$ps (i) and $t = 65.9\,$ps (j). (k) The circles show the line profiles of (i) and (j) taken at $x = -1.9\,\mu$m (shown by the dashed lines). The solid lines are the fits by the convolution of a Gaussian function with $\cos(ky+\phi)$ resulting in a $(0.78 \pm 0.02) \times \pi$ phase difference between the two fits.

arrays at two different array parameters (separation). Observation of dark and bright fringes at the same energy as the condensates themselves indicates that the condensates are phase locked. Constructive interference at the center of the array corresponds to the case where they are all in phase, and destructive interference corresponds to the case where they are out of phase. Fig. 4(c,d) are the GP simulations with random initial phase (see Supp. Info. I B) for 75 realizations, which demonstrate the in-phase (c) and out-of-phase locking of the condensates (d). Here the losses are minimized if either all three neighbors are in phase or if there is a $2\pi/3$ phase difference between the neighbors (see Supp. Info. I C and Supp. Fig. S7). The nontrivial case where there is a $2\pi/3$ phase difference going clockwise or anticlockwise between the neighbors is shown in Fig 4(d). Fig. 4(d) is composed of two topologically different nondegenerate states (shown in panel E and F), with clockwise and anticlockwise $2\pi/3$ phase difference between adjacent neighbors. They correspond to phase vortices with winding numbers of $+1$ or -1 (shown in G and H). Zero intensity in the center

of the system is present for both types of vortices. The condensates switch between all-in-phase to vortex states in a nearly periodic manner as the array parameter changes (see Supp. Fig. S6 for larger separations).

A dynamical transition in time from an all-in-phase state to out-of-phase state can be observed if we keep the array parameter constant and pump the microcavity at higher powers (see Video S3). We pump the cavity at nearly twice the threshold power for condensation. We then interfere the PL from one condensate with that from the other one using the Michelson interferometer. Fig. 4(i,j) show the interferograms at different times when the condensates are all in-phase (i) and when they are out-of-phase (j) (see also Video S4). The line profiles taken from these two interferograms, shown in Fig. 4(k), show that these two states are out of phase by nearly $2\pi/3$ (see also Fig. S8 for the momentum space). The interferometry measurements show that any two neighboring condensates are phase locked. There are two possible stable states in the system: either all condensates are in phase or there is a $\pm 2\pi/3$ phase difference between neighbors, which correspond to clockwise or anticlockwise vortices with ± 1 winding numbers. This dynamical transition from an all in-phase state to a vortex state could also be observed in the momentum space. The transition is caused by the change of condensates outflowing polaritons wavevector as the condensates relax in energy by phonon and exciton scatterings [24].

In conclusion, we studied the phase coupling mechanism of spatially separated polariton condensate pairs. We demonstrated theoretically and experimentally that depending on the wave vector of the outflowing polaritons and the separation of the condensates, a pair of condensates phase synchronize with zero or π phase difference. We explained how losses due to the outflowing polaritons from the condensates are minimized for states with a specific phase difference. Our simulations showed how the spontaneous formation of these vortices is directly related to the spontaneous symmetry breaking and the nonlinearity at the condensation phase transition. We demonstrated the *spontaneous* vorticity resulting from the phase locking of a triangular condensate array. The condensate array spontaneously picks a clockwise or anticlockwise rotating direction due to phase fluctuations at the onset of condensation. Our observations demonstrate the spontaneous symmetry breaking in space in a dissipative bosonic system.

The authors thank Jacqueline Bloch and Aristide Lemaître for the provision of the sample. H.O. and A.V.K would like to thank Jacqueline Bloch for stimulating discussions. P.G.L. and A.V.K. would like to acknowledge the Royal Society and EPSRC through contract EP/F026455/1 for funding. AK acknowledges support from Russian Ministry of Education and Science (contract No.11.G34.31.0067). H.O. acknowledges the use of the IRIDIS High Performance Computing Facility, at the University of Southampton.

I. SUPPLEMENTAL INFORMATION

A. Experimental setup

The details of the microcavity structure could be found in Ref. 25 and the optical setup is shown in detail in Figure S1. The sample was cooled to $\sim$ 10 K using a cold-finger cryostat. The wedged structure of the microcavity allows accurate probing of the cavity and quantum-well detuning (~ -9 meV). The sample was excited nonresonantly into the Bragg mode (~ 0.1 eV above the cavity mode) by 180 fs pulses to make sure that the phase of the excitation laser was lost by multiple relaxations towards the ground state. The condensate lattice was created using a reflective spatial light modulator (SLM) (see Fig. S1b). A high numerical aperture microscope objective (NA = 0.7) focuses the laser ($\lambda \simeq 730$ nm) to a ~ 1.3 μm diameter spot and collects the PL. Imaging the Fourier plane of the emission to a spectrometer allows mapping out of the energy-momentum space.

B. Gross-Pitaevskii equation with Langevin noise

To simulate the stochastic behaviour of our coupled condensates, we use the mean-field Gross-Pitaevskii equation [13] given by

$$i\hbar\frac{\partial\psi(\mathbf{r})}{\partial t} = \left\{E_0 - \frac{\hbar^2}{2m}\nabla^2_{\mathbf{r}} + \frac{i\hbar}{2}[R[n_R(\mathbf{r})] - \gamma_c] + \hbar g|\psi(\mathbf{r})|^2 + V_R(\mathbf{r})\right\}\psi(\mathbf{r}) + f(t), \qquad (2)$$

where $E_0 = \hbar\omega$, m is the effective mass, R is the incoming rate of polaritons from a hot exciton reservoir with a local density of n_R to the condensate, γ_c is the decay rate of polaritons, g is the repulsion constant accounting for polariton-polariton interactions, and V_R is the repulsive potential created by the nonresonant excitation pump. The mean-field repulsive potential V_R is given by the linear expression

$$V_{\mathbf{r}} = \hbar g_R n_R(\mathbf{r}) + \hbar\mathcal{G}P(\mathbf{r}), \qquad (3)$$

where P is the spatially dependent pumping rate of excitons in the reservoir, and g_R and $\mathcal{G}$ are phenomenological constants given by the experimental values. Similar to Ref. 26, $f(t)$ is the Langevin noise given by the correlator

$$\langle f(t)f^*(t')\rangle = \frac{1}{2}Rn_R(\mathbf{r})\delta(t-t'). \qquad (4)$$

Equation 2 is coupled to a rate equation for the reservoir given by:

$$\dot{n}_R(\mathbf{r}) = P(\mathbf{r}) - \gamma_R n_R(\mathbf{r}) - R n_R(\mathbf{r})|\psi|^2. \tag{5}$$

Here, $\gamma_R \gg \gamma_c$ is the decay rate of the excitons, and the last term accounts for depletion of the reservoir due to stimulated emission into the condensate. It is worth mentioning that we do not assume any energy relaxations in any of our simulations.

We use a fifth-order Adams-Bashforth-Moulton predictor-corrector method and take an average for 75 realizations using these parameters: $\hbar R_r = 0.05\,\mu\mathrm{m}^{-2}\mathrm{meV}$, $\hbar g_R = 0$, $\mathcal{G} = 0.0175\,\mu\mathrm{m}^2$, $\hbar g = 0.02\,\mathrm{meV}\mu\mathrm{m}^2$, $\gamma_c = 0.5\,\mathrm{ps}^{-1}$, $\gamma_R = 0.01\,\mathrm{ps}^{-1}$. P is set to give the observed blueshift in the experiment.

C. The dissipative coupling mechanism

To gain more quantitative insight into the dependence of losses on the distance between the pair of condensates we consider the tail $\tilde{\Psi}(\mathbf{r})$ of the condensate wave function in the region away from the excitation spots. In this intercondensate region the polaritons move as free particles and $\tilde{\Psi}(\mathbf{r})$ can be written as superposition of tails from individual condensates. For two condensates of equal size separated by a distance $\mathbf{a}$ we have

$$\tilde{\Psi}(\mathbf{r}) = \frac{1}{\sqrt{2}}\left[\tilde{\psi}\left(\mathbf{r}+\frac{\mathbf{a}}{2}\right) + e^{i\theta}\tilde{\psi}\left(\mathbf{r}-\frac{\mathbf{a}}{2}\right)\right], \tag{6}$$

where θ is the phase difference between the two condensates. The total number of emitted polaritons during the condensate formation is given by

$$I = \int \frac{\mathrm{d}^2k}{(2\pi)^2}|\tilde{\Psi}(\mathbf{k})|^2, \tag{7}$$

$$\tilde{\Psi}(\mathbf{k}) = \int \mathrm{d}^2 r e^{-i\mathbf{k}\cdot\mathbf{r}}\tilde{\Psi}(\mathbf{r}) = \frac{\tilde{\psi}(k)}{\sqrt{2}}\left[e^{i\mathbf{k}\cdot\frac{\mathbf{a}}{2}} + e^{i\theta}e^{-i\mathbf{k}\cdot\frac{\mathbf{a}}{2}}\right]. \tag{8}$$

Due to the interactions between polaritons and the exciton reservoir, the condensate is blueshifted in energy. Outside the pump spot, this potential energy is converted to kinetic energy with a specific in-plane wavevector k_c. As a result, the tail of each condensate is represented in the reciprocal space by a ring with the wave vector k_c satisfying $\omega_{\mathrm{LP}}(k_c) = \omega_c$, where $\omega_{\mathrm{LP}}(k) = \hbar k^2/2m^*$ is the dispersion of the microcavity mode and ω_c is the energy of the condensate [13, 27] (see also Supplementary Fig. S4). Since the condensate wavefunction for outflowing polaritons is mostly composed of those at $k = k_c$, it can be approximated by

$|\tilde{\psi}(k)|^2 \propto \delta(k - k_c)$. Substituting this in Eq. 7 gives the number of emitted polaritons

$$I(k_c a, \theta) \propto [1 + J_0(k_c a)\cos(\theta)], \tag{9}$$

where J_0 is the Bessel function.

It is easy to show that in the general case of N condensates placed at positions $\mathbf{R}_n$ and having phases θ_n the total loss function is given by

$$I \propto \left[1 + \frac{2}{N}\sum_{n,n'} \cos(\theta_n - \theta_{n'}) J_0(k_c|\mathbf{R}_n - \mathbf{R}_{n'}|)\right], \tag{10}$$

where the summation is over all $N(N-1)/2$ pairs. In the case of an equilateral triangular lattice the loss function is minimized when either all three neighbours are in phase or when there is a $2\pi/3$ phase difference between the neighbours. The nontrivial case where there is a $2\pi/3$ phase difference going clockwise or anticlockwise between the neighbours corresponds to two topologically different vortex states with the winding number of +1 or -1.

It is important to note the difference between the dissipative coupling mechanism described here and the "coherent ballistic coupling" mechanism described in the previous publications [15]. The dissipative coupling mechanism causes two condensates with a separation smaller than $L = \pi/k_c$ to couple anti-phase (see Figure S5), whereas the ballistic coupling would always provide for the in-phase coupling.

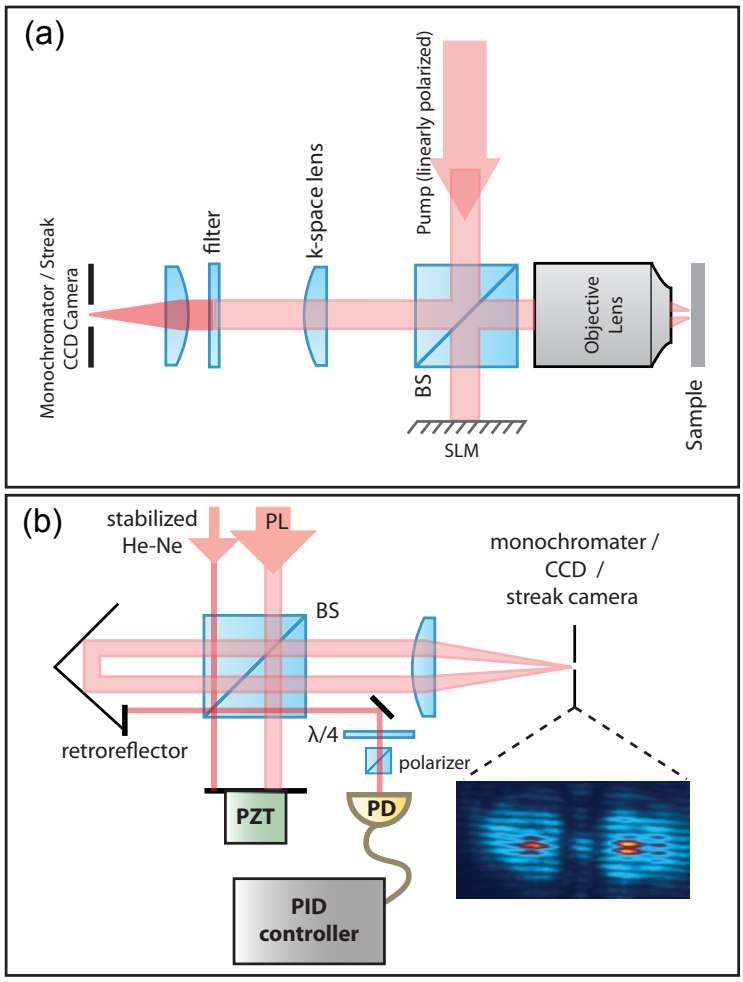

Figure S1. (a) A linearly polarized pump beam is shone on a spatial light modulator (SLM) to generate the pump lattice pattern. The emission is filtered and projected on a monochromator in tandem with a streak camera for time-resolved measurements. (b) Michelson interferometer with a retroreflector in one arm is used to interfere the emission from one condensate with the other. The interference is sent to a streak camera for the time resolution.

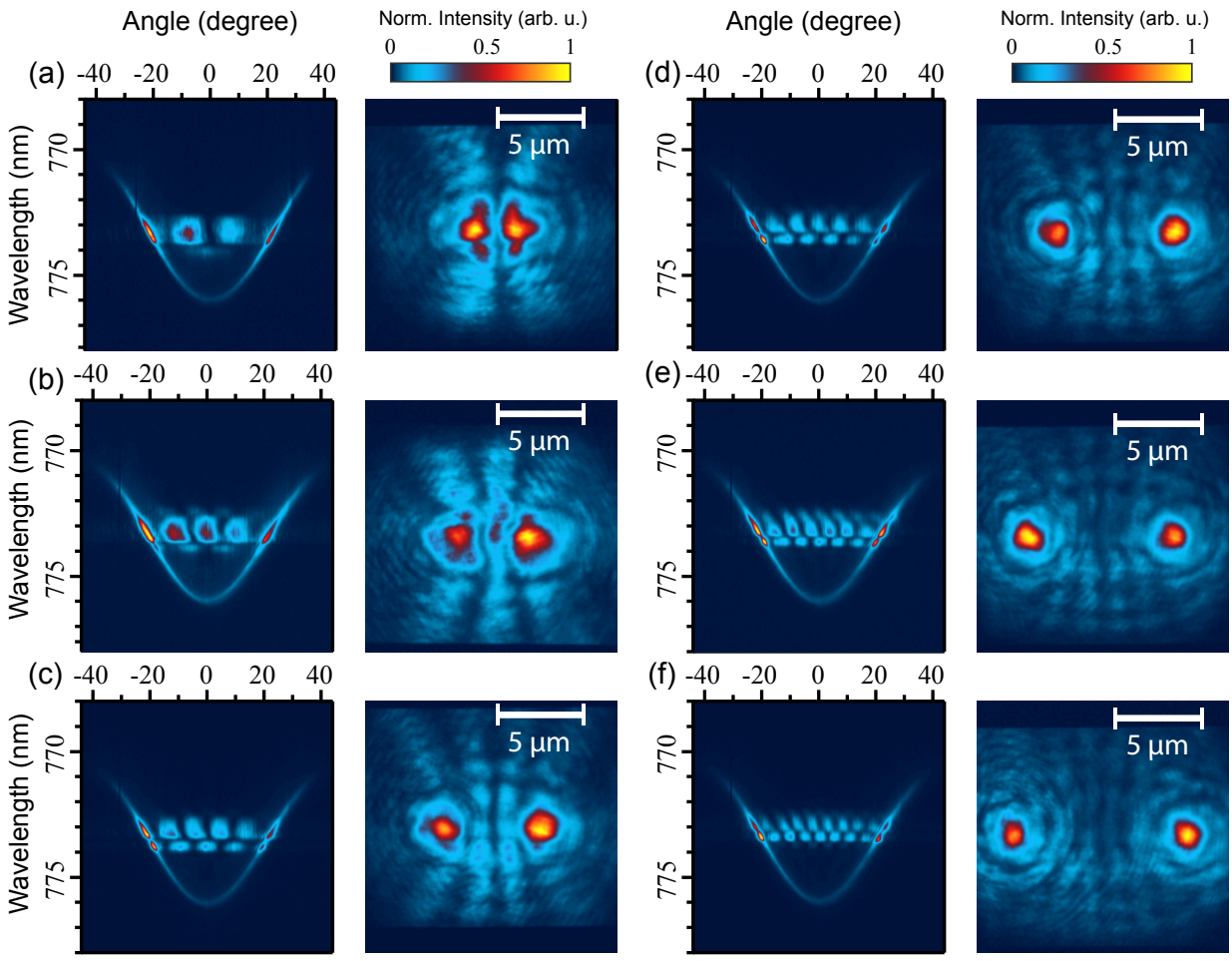

Figure S2. The real space and the momentum space of the two condensates for the separation distance of 2.2 μm (a), 4 μm (b), 5.5 μm (c), 6.5 μm (d), 8.2 μm (e) and 9.7 μm (f) are shown.

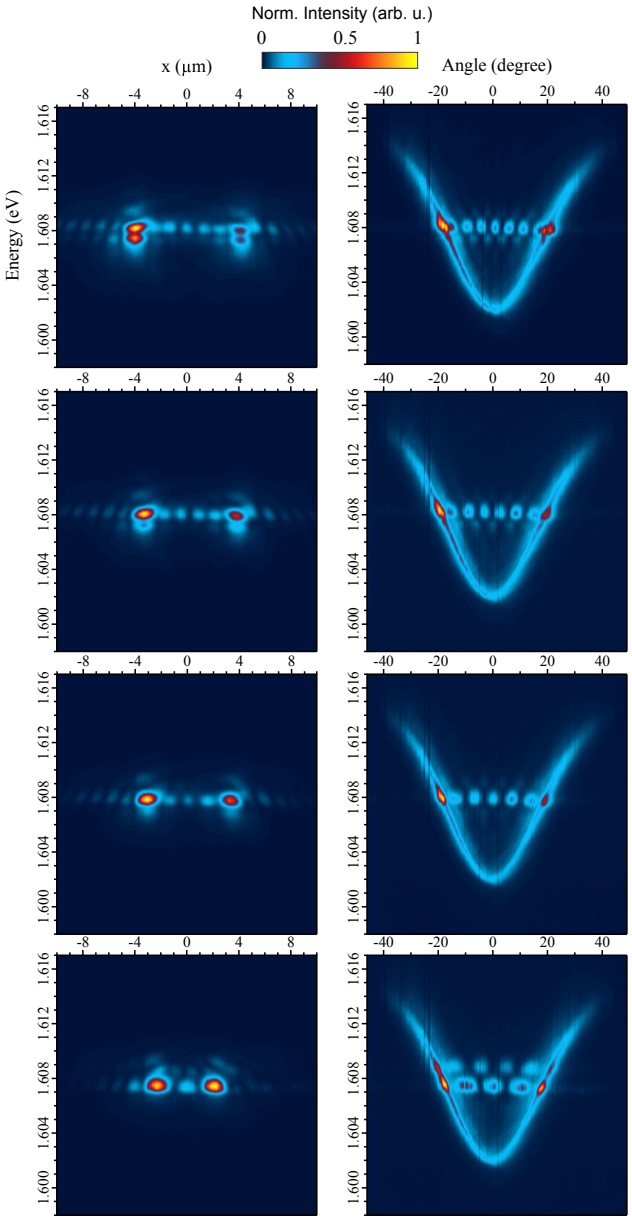

Figure S3. The energy-resolved real space and the momentum space images of the two condensates for different separations are shown. The real spaces images show that the fringes in between the condensates are at the same energy as the condensates are.

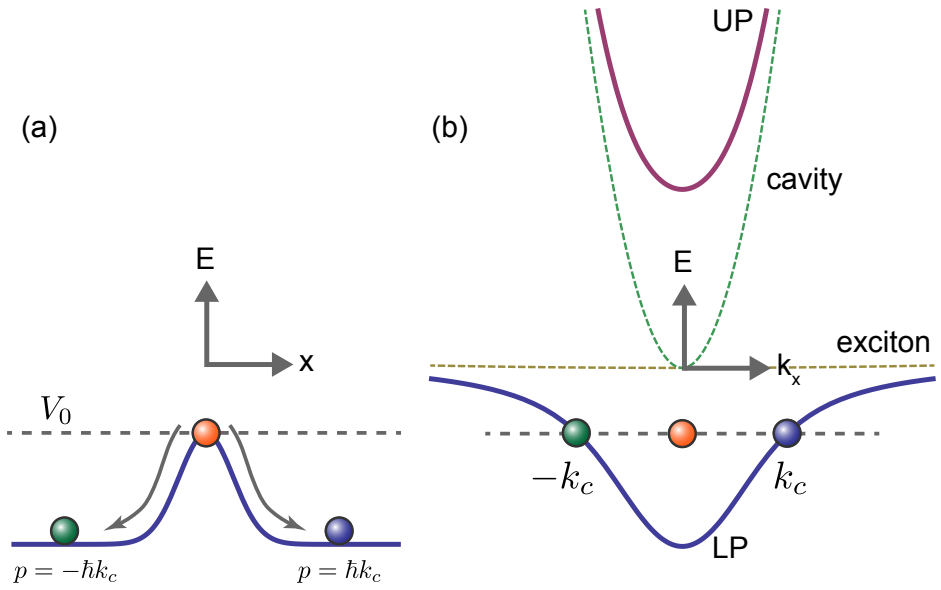

Figure S4. Due to the repulsive interaction of polaritons with background reservoir, the condensate is formed on top of a potential V_0. Polaritons roll down the potential and gain an in-plane momentum $p = \hbar k_c = \sqrt{2mV_0}$.

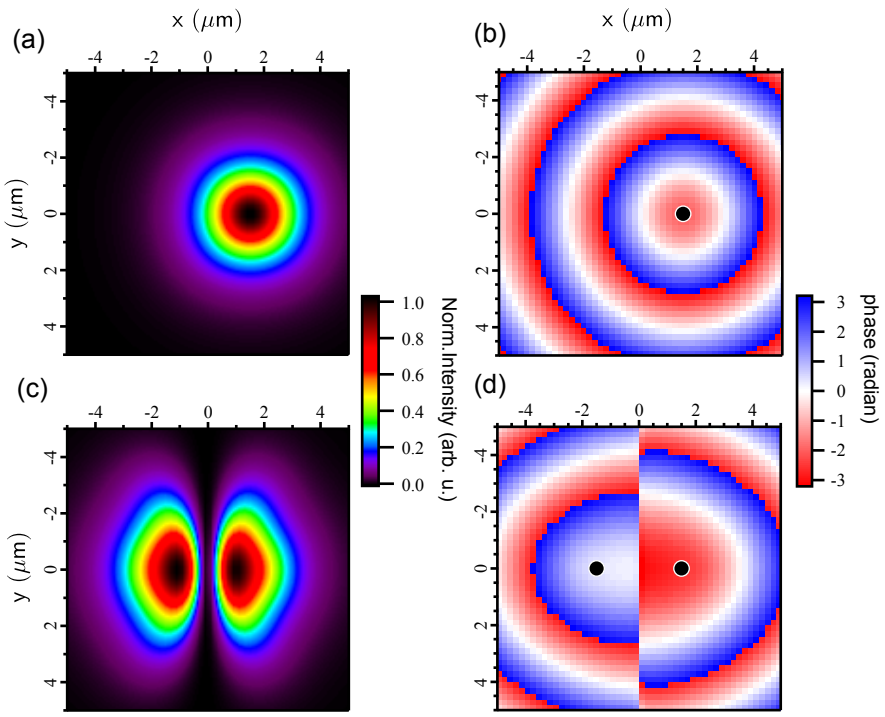

Figure S5. (a,b) The intensity and phase diagram of a single condensate is shown at $x = 1.5\,\mu$m. The flowing polaritons at $x = -1.5\,\mu$m are in-phase with the center of the condensate. (c,d) The intensity and phase diagram of a phase-locked condensate is shown with a separation distance of $3\,\mu$m. The coupled condensates have opposite phases at the centers, opposite to the phase of the flowing polaritons from the other condensate.

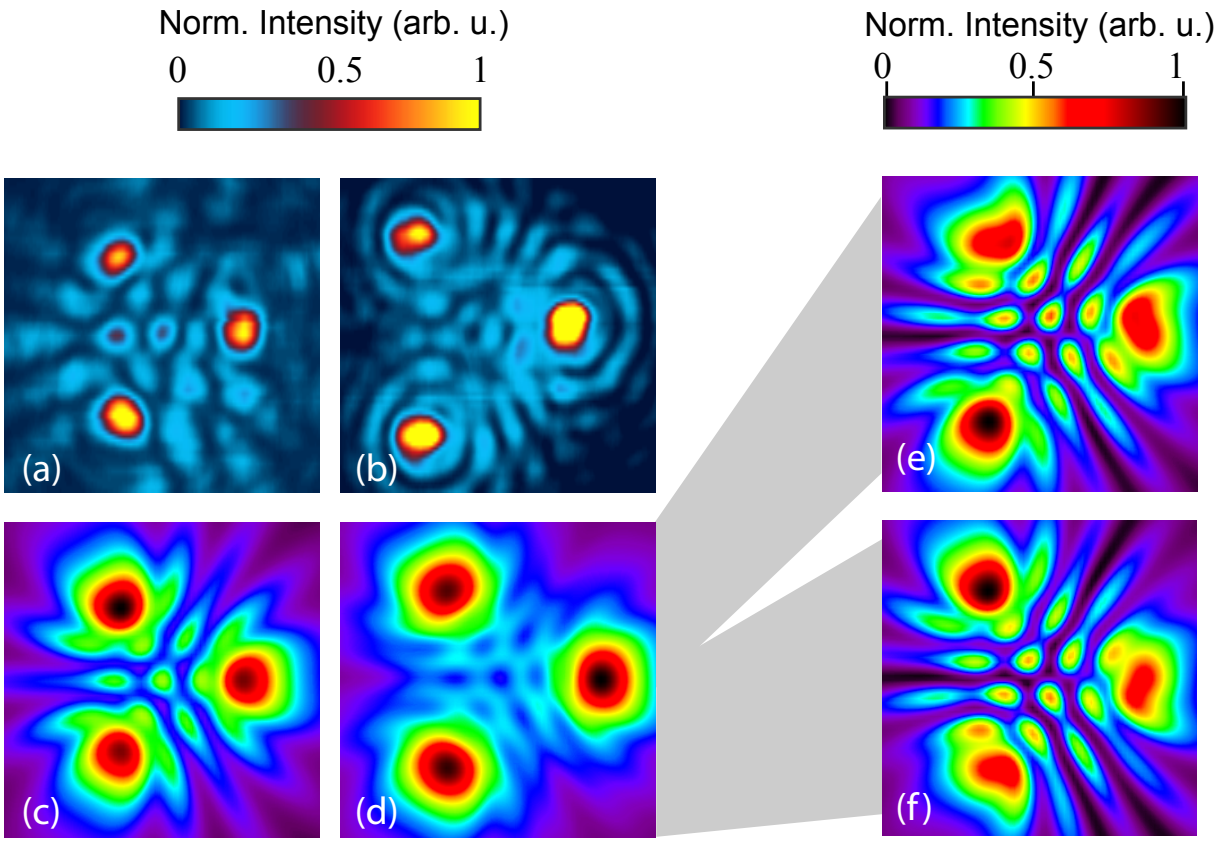

Figure S6. (a,b) The intensity pattern of an all-in-phase triangular lattice, and a vortex state is shown respectively. Th GP simulations for 75 realizations are shown in (c) and (d). Simulations confirm that the vortex states are composed of clockwise and anticlockwise phase vortices shown in (e) and (f).

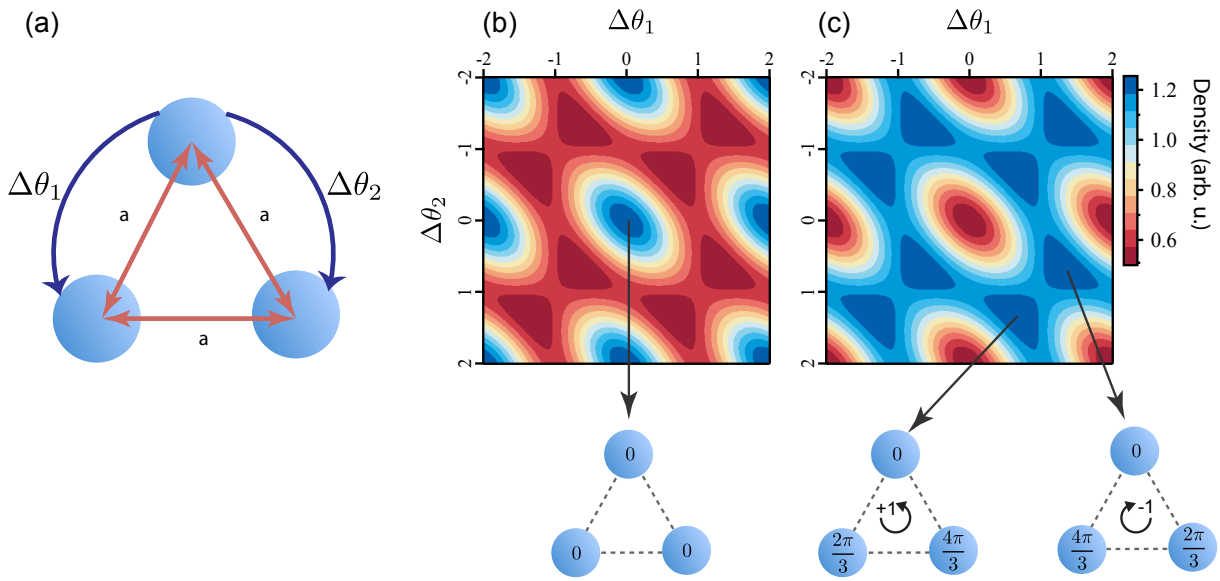

Figure S7. (a) An equilateral triangular lattice with a separation of a between the neighbours and phase difference of $\Delta\theta_1$ and $\Delta\theta_2$ between the neighbours is shown. (b,c) The density function for different phases between the condensates is shown for $k_c = 1\,(\mu\text{m})^{-1}$ and $a = 7\,\mu\text{m}$ (b) and $a = 10\,\mu\text{m}$ (c). The condensates fall into a state with the highest density at the onset of condensation. The maximum density in (c) is composed of two topologically different states, which correspond to clockwise or anticlockwise $2\pi/3$ phase difference between the sites.

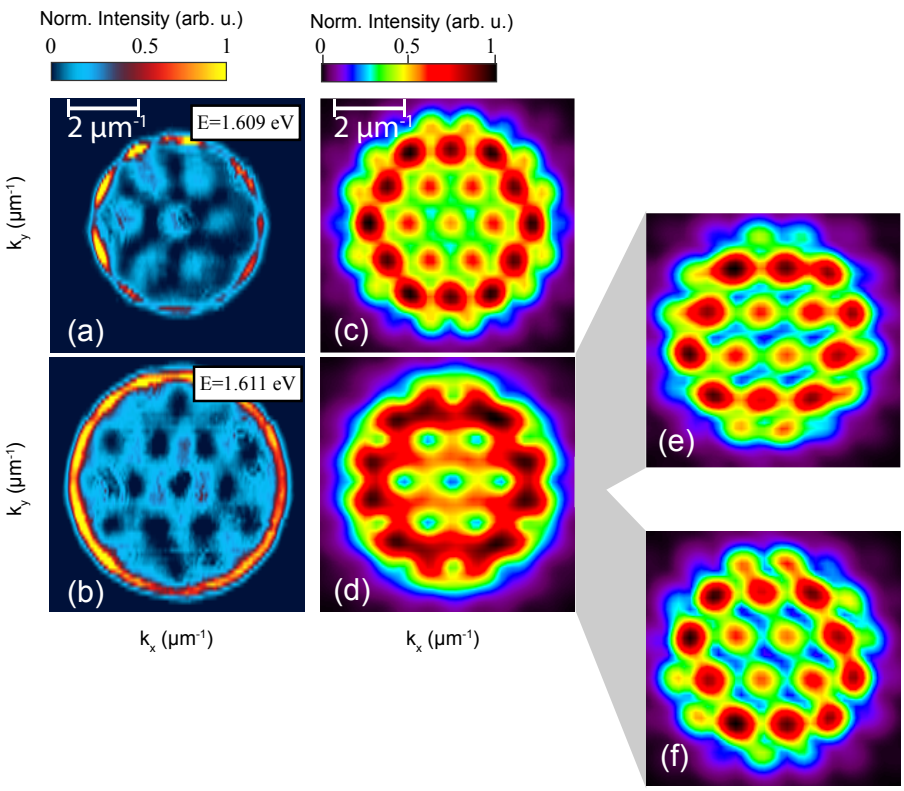

Figure S8. (a,b) The momentum space of a triangular condensate lattice for a lattice constant of 5.5 μm is shown at two different energies, and wavevectors. (a) corresponds to the case where all three condensates are in phase and (b) shows the case where they are in a mixture of clockwise and anticlockwise vortex states with winding numbers of ± 1. (c,d) The GP simulations with Langevin noise with 75 realizations are shown for a separation of 6.5 μm (c) and 5.5 μm (d). (e,f) The simulations show that the honeycomb pattern observed in (d) is indeed a mixture of clockwise (e) and anticlockwise (f) vortex states where the phase difference between neighbors is $2\pi/3$.

* correspondence address: hamid.ohadi@soton.ac.uk

[1] A. V. Kavokin, J. Baumberg, G. Malpuech, and F. P. Laussy, *Microcavities* (Oxford Univ. Press, Oxford, 2007).

[2] J. Kasprzak, M. Richard, S. Kundermann, A. Baas, P. Jeambrun, J. M. J. Keeling, F. M. Marchetti, M. H. Szymańska, R. André, J. L. Staehli, V. Savona, P. B. Littlewood, B. Deveaud, and L. S. Dang, Nature **443**, 409–14 (2006).

[3] R. Balili, V. Hartwell, D. Snoke, L. Pfeiffer, and K. West, Science **316**, 1007 (2007).

[4] H. Deng, G. Weihs, C. Santori, J. Bloch, and Y. Yamamoto, Science **298**, 199 (2002).

[5] C. Schneider, A. Rahimi-Iman, N. Y. Kim, J. Fischer, I. G. Savenko, M. Amthor, M. Lermer, A. Wolf, L. Worschech, V. D. Kulakovskii, I. A. Shelykh, M. Kamp, S. Reitzenstein, A. Forchel, Y. Yamamoto, and S. Höfling, Nature **497**, 348 (2013).

[6] D. Snoke, Science **298**, 1368 (2002), PMID: 12434051.

[7] J. Baumberg, A. Kavokin, S. Christopoulos, A. Grundy, R. Butté, G. Christmann, D. Solnyshkov, G. Malpuech, G. Baldassarri Höger von Högersthal, E. Feltin, J. F. Carlin, and N. Grandjean, Physical Review Letters **101**, 136409 (2008).

[8] H. Ohadi, E. Kammann, T. C. H. Liew, K. G. Lagoudakis, A. V. Kavokin, and P. G. Lagoudakis, Physical Review Letters **109**, 016404 (2012).

[9] J. Kasprzak, D. D. Solnyshkov, R. André, L. S. Dang, and G. Malpuech, Physical Review Letters **101**, 146404 (2008).

[10] K. B. Davis, M. O. Mewes, M. R. Andrews, N. J. van Druten, D. S. Durfee, D. M. Kurn, and W. Ketterle, Physical Review Letters **75**, 3969–3973 (1995).

[11] M. H. Anderson, J. R. Ensher, M. R. Matthews, C. E. Wieman, and E. A. Cornell, Science **269**, 198 (1995).

[12] M. Richard, J. Kasprzak, R. Romestain, R. André, and L. S. Dang, Physical Review Letters **94**, 187401 (2005).

[13] M. Wouters, I. Carusotto, and C. Ciuti, Physical Review B **77**, 115340 (2008).

[14] E. Wertz, L. Ferrier, D. D. Solnyshkov, R. Johne, D. Sanvitto, A. Lemaître, I. Sagnes, R. Grousson, A. V. Kavokin, P. Senellart, G. Malpuech, and J. Bloch, Nature Physics **6**, 860 (2010).

[15] G. Tosi, G. Christmann, N. G. Berloff, P. Tsotsis, T. Gao, Z. Hatzopoulos, P. G. Savvidis, and J. J. Baumberg, Nature Communications **3**, 1243 (2012).

[16] This pattern may look similar to the work reported in Ref. 28 but the physics behind the observed patterns is different in these two works. In our case it is because of the interference of two phase-locked sources rather than the confinement of the wave function in a parabolic

potential. This is very clear as our energy resolved real-space images show that the fringes are at the same energy as the condensates are (see Supp. Fig. S3). Also all real-space images shown in Fig. 4 are tomography images taken at the same energy as the condensates.

[17] K. G. Lagoudakis, B. Pietka, M. Wouters, R. André, and B. Deveaud-Plédran, Physical Review Letters **105**, 120403 (2010).

[18] A. Askitopoulos, H. Ohadi, A. V. Kavokin, Z. Hatzopoulos, P. G. Savvidis, and P. G. Lagoudakis, Physical Review B **88**, 041308 (2013).

[19] I. L. Aleiner, B. L. Altshuler, and Y. G. Rubo, Physical Review B **85**, 121301 (2012).

[20] C. Huygens, in *letter 1338 to Sir Robert Moray (27 Feb 1665) in Oeuvres complètes de Christiaan Huygens.*, Vol. 5 (La HayeM. Nijhoff, 1665) pp. 246–249, see also letter 1335 (Huygens to his father, 26 Feb 1665), pp. 243-244.

[21] M. Bennett, M. F. Schatz, H. Rockwood, and K. Wiesenfeld, Proceedings of the Royal Society of London. Series A: Mathematical, Physical and Engineering Sciences **458**, 563 (2002).

[22] G. Weinreich, The Journal of the Acoustical Society of America **62**, 1474 (1977).

[23] G. S. Smith, European Journal of Physics **31**, 819 (2010).

[24] M. Wouters, T. C. H. Liew, and V. Savona, Physical Review B **82**, 245315 (2010).

[25] E. Kammann, H. Ohadi, M. Maragkou, A. V. Kavokin, and P. G. Lagoudakis, New Journal of Physics **14**, 105003 (2012).

[26] D. Read, T. C. H. Liew, Y. G. Rubo, and A. V. Kavokin, Physical Review B **80**, 195309 (2009).

[27] E. Kammann, T. C. H. Liew, H. Ohadi, P. Cilibrizzi, P. Tsotsis, Z. Hatzopoulos, P. G. Savvidis, A. V. Kavokin, and P. G. Lagoudakis, Physical Review Letters **109**, 036404 (2012).

[28] G. Tosi, G. Christmann, N. G. Berloff, P. Tsotsis, T. Gao, Z. Hatzopoulos, P. G. Savvidis, and J. J. Baumberg, Nat Phys **8**, 190 (2012).